Fracture Permeability Enhancement During Fluid Injection Modulated by Pressurization Rate and Surface Asperities

Yinlin Ji, Wei Zhang, Hannes Hofmann, Frédéric Cappa, Supeng Zhang

Geophysical Research Letters

RESEARCH LETTER
10.1029/2023GL104662

Fracture Permeability Enhancement During Fluid Injection Modulated by Pressurization Rate and Surface Asperities

Yinlin Ji[1], Wei Zhang[2], Hannes Hofmann[1,3], Frédéric Cappa[4], and Supeng Zhang[1,5]

[1]Helmholtz Centre Potsdam GFZ German Research Centre for Geosciences, Potsdam, Germany, [2]School of Petroleum Engineering, China University of Petroleum (East China), Qingdao, China, [3]Institute of Applied Geosciences, Technische Universität Berlin, Berlin, Germany, [4]Université Côte d'Azur, CNRS, Observatoire de la Côte d'Azur, IRD, Sophia Antipolis, France, [5]Key Laboratory of Shale Gas and Geoengineering, Institute of Geology and Geophysics, Chinese Academy of Sciences, Beijing, China

Abstract We present a series of controlled fluid injection experiments in the laboratory on a pre-stressed natural rough fracture with a high initial permeability (~10^{-13} m^2) in granite using different fluid pressurization rates. Our results show that fluid injection on a fracture with a slight velocity-strengthening frictional behavior exhibits dilatant slow slip in association with a permeability increase up to ~41 times attained at the maximum slip velocity of 0.085 mm/s for the highest-rate injection case. Under these conditions, the slip velocity-dependent change in hydraulic aperture is a dominant process to explain the transient evolution of fracture permeability, which is modulated by fluid pressurization rate and fracture surface asperities. This leads to the conclusion that permeability evolution can be engineered for subsurface geoenergy applications by controlling the fluid pressurization rate on slowly slipping fractures.

Plain Language Summary Understanding the evolution of fracture permeability during hydraulic stimulation of subsurface reservoirs is the key to characterizing fluid transport and formulating strategies to limit induced seismicity. Accordingly, there is a significant interest in deciphering how the fluid pressurization rate, a constitutive operational parameter during injection, influences the transient permeability change during fracture slip. We conducted a series of experiments in the laboratory using different fluid pressurization rates on a natural rough fracture in granite under a pre-stressed state. The fracture had a high initial permeability. Our findings show that when fluid is injected into a fracture with a slight velocity-strengthening frictional behavior, it causes slow slipping with significant permeability enhancement. The change in hydraulic aperture caused by slip velocity is the main reason for the temporary change in permeability, and this effect is modulated by fluid pressurization rate and fracture surface irregularities. Our results suggest that we can modulate the permeability of subsurface geoenergy reservoirs by controlling the fluid pressurization rate on slowly slipping fractures.

Key Points:

- We conducted fluid injection experiments on a pre-stressed natural rough fracture in granite at different pressurization rates
- The velocity-strengthening fracture exhibits slow slip accompanied by a significant increase in permeability during fluid injection
- Transient fracture permeability is controlled by injection-induced slip velocity, modulated by pressurization rate and surface asperities

Supporting Information:

Supporting Information may be found in the online version of this article.

Correspondence to:

Y. Ji,
yinlinji@gfz-potsdam.de

Citation:

Ji, Y., Zhang, W., Hofmann, H., Cappa, F., & Zhang, S. (2023). Fracture permeability enhancement during fluid injection modulated by pressurization rate and surface asperities. *Geophysical Research Letters*, *50*, e2023GL104662. https://doi.org/10.1029/2023GL104662

Received 22 MAY 2023
Accepted 7 SEP 2023

Author Contributions:

Conceptualization: Yinlin Ji
Data curation: Yinlin Ji
Formal analysis: Yinlin Ji
Funding acquisition: Hannes Hofmann
Methodology: Yinlin Ji
Software: Wei Zhang, Supeng Zhang
Validation: Hannes Hofmann, Frédéric Cappa
Writing – original draft: Yinlin Ji
Writing – review & editing: Yinlin Ji, Hannes Hofmann, Frédéric Cappa

1. Introduction

Subsurface hydraulic stimulations for geoenergy development aim to increase the reservoir permeability via hydro-fracturing and hydro-shearing processes. Examples of such applications include fluid injection for enhanced geothermal systems (Li & Zhang, 2023; Olasolo et al., 2016; Schoenball et al., 2020), as well as oil and shale gas exploitation (Das & Zoback, 2013; Kim & Moridis, 2015). Rock fractures provide preferential fluid pathways that can transport thermal energy and shale oil and gas. A wealth of evidence from laboratory and field experiments suggests that hydro-shearing, which involves injection-induced slip along fractures and faults, is the primary contributor to enhancing reservoir permeability even when no proppants or acids are used (Barton et al., 2009; Cappa, Guglielmi, & De Barros, 2022; Cappa, Guglielmi, Nussbaum, et al., 2022; Guglielmi et al., 2015; Ishibashi et al., 2018; Jalali et al., 2018), but this process may also lead to unintentional and undesired large-magnitude induced seismic events ($M_w > 3$) (Ji, Hofmann, Duan, & Zang, 2022; Keranen & Weingarten, 2018; Schultz et al., 2020; Zang et al., 2014). Thus, the ability to predict the transient permeability evolution of individual fractures is the key to accurately estimating fluid flow and reservoir response with controlled seismicity during injection.

Permeability measurements in conventional displacement-driven shear experiments in the laboratory have shown that the fracture permeability evolution can be influenced by the surface roughness (Fang, Elsworth, Ishibashi, & Zhang, 2018; Wu et al., 2017), mineral composition (Fang, Elsworth, Wang, & Jia, 2018; Fang et al., 2017),

stress state (Gutierrez et al., 2000; Rutter & Mecklenburgh, 2018), slip direction (Okazaki et al., 2013; Rutter & Mecklenburgh, 2017), slip velocity (Fang et al., 2017; Ishibashi et al., 2018), as well as slip mode (Almakari et al., 2020; Rutter & Mecklenburgh, 2018). Meanwhile, for injection-induced fracture permeability evolution, several experimental studies have shown that the fracture permeability increases with decreasing effective normal stress (i.e., increasing fluid pressure) and dilatant slip has been identified as the key mechanism responsible for permeability enhancement. Particularly, the fracture permeability in granite shows an irreversible enhancement by self-propping shear activated by fluid pressurization under typical deep geothermal stress conditions (Ye & Ghassemi, 2018), which is more pronounced at lower confining pressures (Almakari et al., 2020). More recently, the transient permeability enhancement of slowly slipping faults activated by fluid injection in underground galleries is found to be controlled by the changes in slip velocity (Cappa, Guglielmi, & De Barros, 2022) with increasing fluid pressure, congruent with the laboratory-derived semi-analytical model relating slip velocity and aperture change (Fang et al., 2017; Samuelson et al., 2009). However, although these previous experiments provide important insights into the physics of fluid flow and shear slip in fractures, the effects of fluid pressurization rate and fracture surface asperities on transient permeability change during fracture slip remain poorly constrained.

Here, we performed a series of controlled laboratory fluid injection experiments on a pre-stressed natural rough fracture in granite to explore the effects of fluid pressurization rate and fracture surface asperities on transient fracture permeability change. Three fluid injection experiments with different fluid pressurization rates were conducted consecutively under the same initial stress conditions. Results give new insights into how the fluid pressurization rate and fracture surface asperities control the transient fracture permeability change during injection-induced fracture slip. To the best of our knowledge, this work is the first to link the fluid pressurization rate and fracture surface asperities with transient fracture permeability enhancement using controlled laboratory-sized experiments (cf., Ji, Hofmann, Duan, & Zang, 2022; Zhuang & Zang, 2021).

2. Materials and Methods

The fluid injection experiments were performed at room temperature (~22°C) on a naturally formed rough fracture in granite (Figure 1a) using the triaxial shear-flow setup (Figure 1b) in the MTS 815 rock mechanics test system (Text S1 in Supporting Information S1). The Bukit Timah granite sample was cored from a depth of approximately 10 m in central Singapore, Asia, which is a potential geothermal reservoir rock. The physical, mechanical, and hydraulic properties of the granite (Ji, 2020; Peng et al., 2017) are summarized in Table S1 of the Supporting Information S1. We selected a 50-mm-diameter core sample containing a pre-existing sealed natural fracture and cut it to ~123.8 mm length. We then compressed the sample until it failed along the fracture plane at 20 MPa confining pressure by advancing the axial piston at a velocity of 1 μm/s, producing a cylindrical sample containing a natural rough fracture inclined 27° to the core axis. The minor and major axes of the elliptical planar fracture measure 110 and 50 mm, respectively, resulting in a fracture area of 4,320 mm^2. Upon visual inspection of the fracture surface, it appears that the fracture is most likely a magma cooling-induced break of the surrounding granite without obvious mineral intrusion (Zhao, 1997). Moreover, the fracture is not filled with granular material. Analysis of the fracture surface topography using a structured light scanner (Model No.: DAVID SLS-3) indicates a joint roughness coefficient (JRC) of 12.5 (Table S2 in Supporting Information S1 and the accompanying notes). This JRC value corresponds to a "rough" fracture, as classified by Barton and Choubey (1977). Two vertical boreholes with a diameter of ~2 mm were drilled at the short edge of each sample half to facilitate the fluid communication between the endcap and the fracture surface. Filter paper with a pore size of 0.45 μm was inserted between endcaps and sample ends to inhibit the possible contamination of fluid pipes by the produced wear particles. The sample was secured on the endcaps by two layers of Teflon jacket to exclude confining oil. The favorable angle of 27° prevents the fracturing of the granite matrix during axial loading (Brady & Brown, 2013; Ji, 2020). The permeability contrast between rock matrix (~1.3×10^{-18} m^2, Table S1 in Supporting Information S1) and fracture (~1.0×10^{-13} m^2, Text S1 and Table S3 in Supporting Information S1) ensures that the fluid only flows through the fracture during the experiments.

The sample was vacuum-saturated with distilled water for ~24 hr before the experiments. Afterward, the confining pressure was first repeatedly cycled between 2 and 11 MPa to stabilize the sample by eliminating any misalignment of the two rock blocks (cf., Kohli & Zoback, 2013; Ji, Kluge, et al., 2022). Then, under 2 MPa confining pressure, pressurized distilled water was injected directly into the fracture to reach a fluid pressure

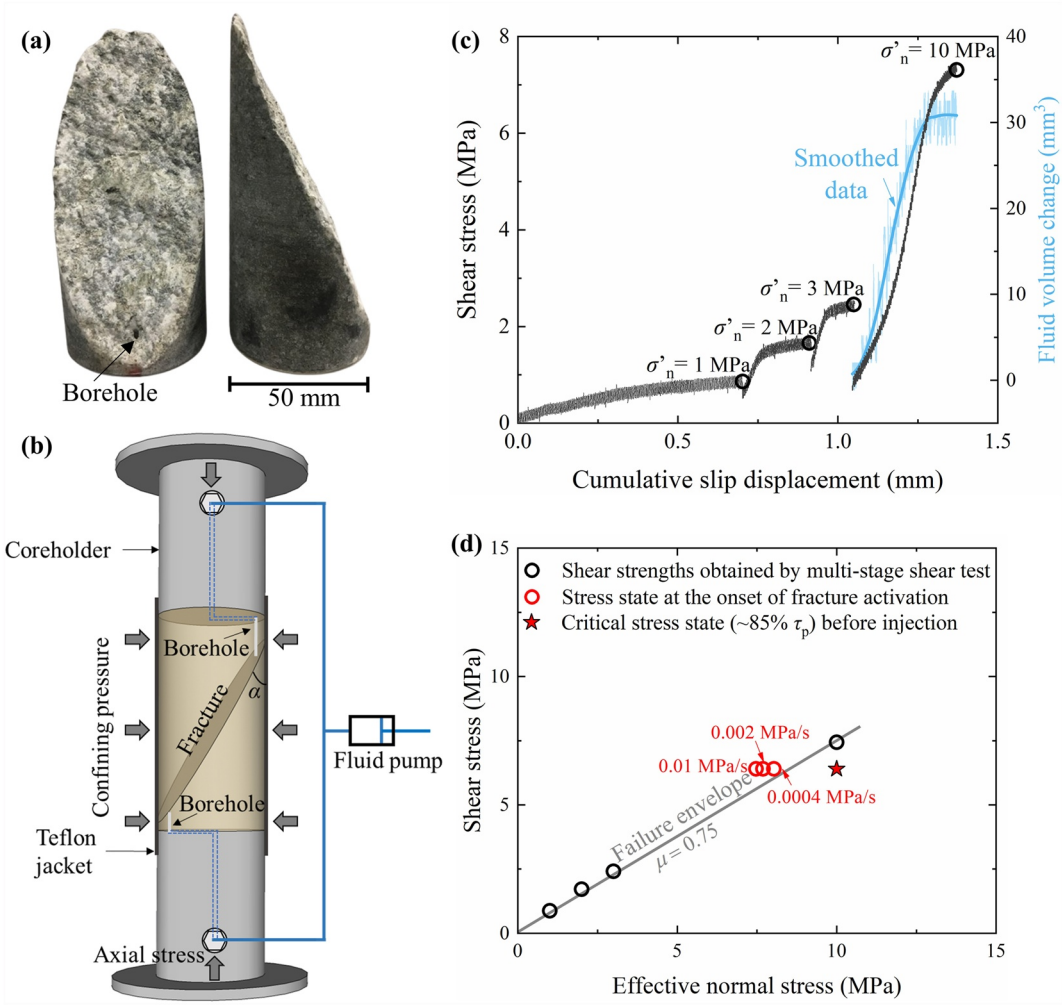

Figure 1. Experimental material, setup, loading procedure and failure envelope. (a) Natural rough fracture in Bikit Timah granite with a joint roughness coefficient of 12.5. (b) Triaxial shear-flow setup, where $\alpha = 27°$ is the fracture inclination angle with respect to the sample axis. (c) Multi-stage shear loading before fluid injection to obtain the peak shear strengths (τ_p, denoted by black open circles) under 1, 2, 3, and 10 MPa effective normal stresses (σ'_n). At 10 MPa effective normal stress (constant fluid pressure = 1 MPa), the fluid volume change first increases dramatically due to shear dilation, and it remains unchanged after reaching the yield shear stress of ~6.6 MPa, suggesting that the steady-state fracture aperture becomes relatively constant with increasing slip displacement beyond this point. (d) Mohr-coulomb failure envelope of the fracture in terms of shear stress as a function of effective normal stress obtained from the multi-stage shear test. The five-pointed star and red open circles represent the stress states of the fracture before fluid injection (~85% τ_p and $\sigma'_n = 10$ MPa) and at the onset of fracture activation, respectively. The apparent steady-state friction coefficient (μ) of the fracture is estimated as $\mu = 0.75$ with zero cohesion. The stress states at the onset of fracture activation are generally compatible with the Mohr-coulomb failure envelope, indicating the near-uniform distribution of fluid pressure on the fracture surface.

of 1 MPa, and maintained constant until the full saturation of the sample, signified by negligible fluid volume intake. After full saturation, we first obtained the apparent steady-state friction coefficient (μ) of the fracture by conducting a multi-stage shear test under an effective normal stress (i.e., total normal stress σ_n minus fluid pressure p, $\sigma'_n = \sigma_n - p$) of 1, 2, 3, and 10 MPa (Figures 1c and 1d) each at a constant fluid pressure of 1 MPa and an axial displacement rate of 1 μm/s. We then reduced the shear stress to ~85% peak shear strength under 11 MPa normal stress and 1 MPa fluid pressure on the fracture. Following that, we held the shear and normal stresses on the fracture constant (the five-pointed star in Figure 1d), and water was injected at a constant pressurization rate through the two boreholes, which were connected to the same fluid pump, to induce the opening and slip of the pre-stressed fracture. The schematic of the stress paths during mechanical loading and fluid injection shows how the stress state approaches the Mohr-Coulomb failure envelope (Figure S1 in Supporting Information S1).

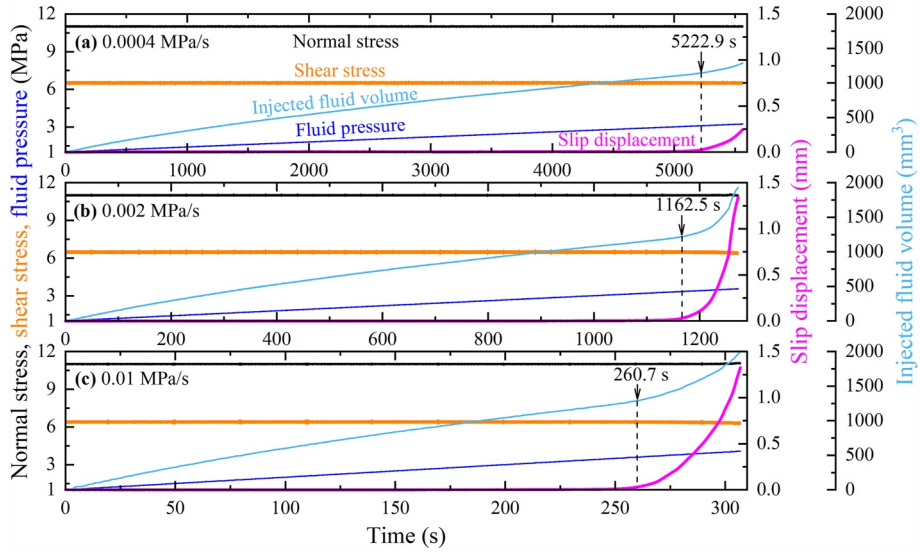

Figure 2. Temporal changes of hydromechanical parameters during fluid injection experiments. Time-dependent evolution of normal stress, shear stress, fluid pressure, slip displacement and injected fluid volume in the fluid injection experiments at a fluid pressurization rate of (a) 0.0004, (b) 0.002, and (c) 0.01 MPa/s. The initiation of fracture activation is signified by the increase of slip displacement along the fracture. The injected fluid volume first increases near linearly with time followed by abrupt increases. The time when the increase of injected fluid volume deviates from the linear trend is roughly the time at the onset of fracture activation (see black arrows and dashed lines). Note that the slip displacement is offset to zero at the start of fluid pressurization in each experiment.

A sequence of three fluid injection experiments with different fluid pressurization rates of 0.0004, 0.002, and 0.01 MPa/s were performed on the same fracture under the same initial stress conditions. The three pressurization rates were carefully chosen to achieve a balance: they were neither excessively high, ensuring a consistently near-uniform fluid pressure distribution on the fracture (cf., Passelègue et al., 2018), nor excessively low, enabling the observation of fracture response to fluid injection within a reasonable testing time. The time interval between two successive experiments was ~20 min to ensure that the fracture was in a stabilized hydromechanical state (i.e., equilibrium) before the subsequent fluid injection. In addition, prior to each fluid injection experiment, we measured the steady-state fracture permeability using the steady state flow technique by imposing a constant upstream fluid pressure of 1 MPa through the bottom borehole with the downstream opening to the atmosphere and measuring the resulting flow rate (Text S1 in Supporting Information S1).

3. Results

3.1. Frictional Strength and Fracture Deformation in the Experiments

The three peak shear strengths (τ_p) obtained from the multi-stage shear test were used to construct the Mohr-Coulomb failure envelope, yielding an apparent steady-state friction coefficient of 0.75 by setting a zero cohesion (Figure 1d), generally compatible with Byerlee's rule of rock friction (Byerlee, 1978). In the subsequent three fluid injection experiments, the normal stress and shear stress were held constant at 11 and 6.41 MPa (~85% τ_p), respectively (Figure 2). The fracture was activated and the slip was initiated once the fluid pressure approached a critical value. In our experiments, the critical activation fluid pressure p_{ff} is predicted as 3.42 MPa based on the Mohr-Coulomb failure criterion incorporating the effective stress law, which is roughly consistent with the laboratory measurements (Figure 1d; Table S3 and Text S2 in Supporting Information S1), indicative of a near-uniform fluid pressure distribution over the fracture surface (Ji et al., 2020; Passelègue et al., 2018; Rutter & Hackston, 2017). The near-homogeneous fluid pressure distribution on the fracture surface is also confirmed by the short characteristic diffusion time (Mavko et al., 2009) (Text S2 in Supporting Information S1).

In the fluid injection experiments, the normal stress and shear stress remain unchanged under servocontrol during fluid pressurization (Figure 2). The fluid pressure is elevated from 1 MPa in all the three fluid injection experiments. Fluid pressurization of the fracture requires injection of fluid volume from the pump, according to the

compression-induced pressurization principle of fluids (Ji, Kluge, et al., 2022; Kestin, 1979). Particularly, the elevation of fluid pressure is linearly correlated with the increase of injected fluid volume when the sample volume is constant, and thus any changes in sample volume result in variations of the injected fluid volume (cf., Ashman & Faulkner, 2023; Samuelson et al., 2009). The slip displacement starts to increase when the fluid pressure reaches the critical activation fluid pressure. The injected fluid volume increases near linearly before fracture activation, suggesting that the injected fluid volume mainly serves to compensate for the compressed volume during the fluid pressure increase. Hence, the elastic normal opening of the fracture induced by the reducing effective normal stress is negligible as previously observed in other experimental studies (cf., Cappa, Guglielmi, & De Barros, 2022; Guglielmi et al., 2015). This may be due to the small increase of fluid pressure (<2.51 MPa) as the fracture is already primed close to failure, and the high normal stiffness of the fracture in granite (in the order of ∼100 MPa/mm for clean natural fractures in granite, Zangerl et al., 2008). In particular, the maximum volume increase associated with elastic fracture opening induced by reducing effective normal stress is estimated as small as ∼108 mm^3, which is smaller than 0.09 times the total injected fluid volume upon fracture activation (Table S3 in Supporting Information S1). Upon fracture activation, the increase of injected fluid volume starts to deviate from the linear trend at the time of 5,222.9, 1,162.5, and 260.7 s at the pressurization rate of 0.0004, 0.002, and 0.01 MPa/s, respectively, and the excessive injected fluid volume is primarily accommodated by the fracture dilation associated with shear slip (Figure 2) (Ji et al., 2019; Li et al., 2021). At the termination of fluid injection, the fracture slips by 0.24, 1.34, and 1.25 mm in the fluid injection experiments at a pressurization rate of 0.0004, 0.002, and 0.01 MPa/s, respectively.

At the same amount of slip displacement change, the slip velocity generally increases with a higher fluid pressurization rate with some large fluctuations especially at larger slip displacement (Figure S2 in Supporting Information S1). The peak slip velocity increases by ∼15 times at 0.24 mm slip displacement change by elevating the pressurization rate from 0.0004 to 0.01 MPa/s. The increased slip velocity at higher-rate fluid pressurization cases is ascribed to the larger strength deficit relative to the applied shear stress: the higher the fluid pressurization rate, the faster rate of reduction in effective normal stress and thereby shear strength, and the larger the slip acceleration, resulting in a higher slip velocity. The fluctuation of slip velocity with increasing slip displacement could be attributed to various sizes and strengths of surface asperities (cf., Goebel et al., 2012; Xu et al., 2023; Ye & Ghassemi, 2020).

The maximum slip velocity in our fluid injection experiments is smaller than 0.1 mm/s (Table S3 in Supporting Information S1), suggesting that the injection-induced slow slip is mainly aseismic (Tinti et al., 2016). This is further confirmed by the evolution of the apparent friction coefficient (Figure S3 in Supporting Information S1), measured as the ratio of the shear stress to effective normal stress, as a function of the logarithm of the slip velocity ($\ln(v/v_0)$, where v is the slip velocity and v_0 is the background slip velocity before fracture activation) (Guglielmi et al., 2015; Marone, 1998) (Table S4 in Supporting Information S1). On average, the fracture exhibits a slight velocity-strengthening frictional behavior, marked by a positive slope in the friction coefficient-versus-$\ln(v/v_0)$ plots in the three injection experiments (Figure S3 in Supporting Information S1). This is congruent with previous laboratory results suggesting that rough fractures exhibit more positive velocity-strengthening frictional behavior than smooth fractures (Fang, Elsworth, Ishibashi, & Zhang, 2018), a condition facilitating aseismic slow slip upon activation.

3.2. Velocity Dependence of Transient Fracture Permeability

First, by assuming that the excessive injected fluid volume is primarily accommodated by the increased fracture volume due to shear-induced dilation, we can estimate the transient change of hydraulic aperture (Δb) accompanying injection-induced fracture slip from the temporal evolution of the injected fluid volume as (Ji et al., 2019; Li et al., 2021),

$$\Delta b = \frac{\Delta V_f}{A} \tag{1}$$

where ΔV_f is the transient excessive increase of injected fluid volume during dilatant fracture slip relative to that before fracture activation (see Text S3 in Supporting Information S1 for detailed calculations); A is the area of the elliptical fracture. Thus, the result obtained by Equation 1 is volume-based hydraulic aperture change. Note that here we posit that the congruence between alterations in hydraulic aperture and mechanical aperture remains

steadfast, substantiated by prior investigations of permeable fractures within controlled laboratory settings (Fang et al., 2017; Li et al., 2021) and natural field conditions (Cappa, Guglielmi, & De Barros, 2022).

We then used the laboratory-derived semi-analytical model relating slip velocity (v) with aperture (b) (Fang et al., 2017; Samuelson et al., 2009) to model the volume-based aperture in our experiments,

$$\Delta\varepsilon_i = -\Psi \cdot \ln\left[\frac{v_{i-1}}{v_i}\left(1 + \left(\frac{v_i}{v_{i-1}} - 1\right) \cdot e^{-v_i \cdot t_i / D_c}\right)\right] \quad (2)$$

$$b^n_{evo} = b^n_{slip} \prod_{i=0}^{i=n} (1 + \Delta\varepsilon_i) \quad (3)$$

where i is the ith velocity step; $\Delta\varepsilon$ is the dilation parameter; Ψ is the dilation factor; t_i is the time since the ith velocity step; D_c is the critical slip distance; b^n_{evo} and b^n_{slip} are the modeled aperture and slip-dependent aperture at the nth velocity step, respectively.

For the shear test conducted under 11 MPa normal stress and 1 MPa fluid pressure, the fluid volume change indicates that the fracture aperture gradually increases with increasing slip displacement initially because of shear dilation, but remains mostly stable after reaching the yield shear stress of ~6.6 MPa (Figure 1c). Therefore, we assumed that the slip-dependent aperture (b^n_{slip}) stays unchanged at the initial hydraulic aperture (b_0) in each injection case. The validity of this assumption is bolstered by the fact that the steady-state fracture permeability, as measured prior to each injection experiment, remains almost unchanged (Table S3 in Supporting Information S1). Further, because $k = b^2/12$ (Snow, 1969; Witherspoon et al., 1980), the transient permeability change (k/k_0) can be calculated as the square of the ratio between b^n_{evo} and b_0, where k denotes the transient permeability at the nth velocity step (k_n) and k_0 is the initial fracture permeability before activation.

This velocity-dependent fracture permeability model has been successfully used to reproduce the transient permeability change of fractures/faults in the field-scale fluid injection experiments (Cappa, Guglielmi, & De Barros, 2022) and in the lab-scale shear friction experiments (Fang et al., 2017). Based on Equations 2 and 3, the best-fit velocity-dependent aperture models to our experimental aperture data derived from injected fluid volume (Equation 1) were obtained by searching the optimal dilation factor (Ψ) in the range from 0 to 5, and critical slip distance (D_c) from 0.1 to 5,000 μm using the genetic algorithm (Holland, 1992; Zbigniew, 1996) (Text S4 in Supporting Information S1). The root mean square error (RMSE) has a global minimum value at (Ψ = 0.08, D_c = 0.4 μm), (Ψ = 0.93, D_c = 0.16 μm) and (Ψ = 0.84, D_c = 2.74 μm) in modeling the fluid injection experiments at a pressurization rate of 0.0004, 0.002 and 0.01 MPa/s, respectively (Figure S4 in Supporting Information S1). The dilation factors (Ψ) in our best-fit models are comparable to the values obtained in previous studies on laboratory fractures (Fang et al., 2017) and in-situ faults (Cappa, Guglielmi, & De Barros, 2022). Our modeling results seem less sensitive to the critical slip distance (D_c) within a range of less than one order of magnitude around the optimal value. This is presumably because the influence of each velocity step tends to reach the steady state at small optimal D_c (see Equation 2), and thus a small change of D_c around the optimal value may not change much the modeling results.

Figures 3a, 3c, and 3e show that the aperture change calculated using the velocity-dependent aperture model (Equations 2 and 3) demonstrates a satisfactory agreement with the measured aperture change determined from the injected fluid volume (Equation 1), signified by the small RMSE values. Note that the RMSE in the first fluid injection experiment at a rate of 0.0004 MPa/s is ~3 times that of the other two higher-rate counterparts, which may be due to the relatively poor constraint on the model by the short slip displacement and noisy slip velocity data. The transient permeability change (k/k_0) is always larger than unity (Figures 3b, 3d, and 3f) with the maximum value of ~41 attained at the maximum slip velocity of 0.085 mm/s in the highest-rate injection case (Figure 3f), highlighting that the transient fracture permeability accompanying fracture slip is enhanced relative to the initial steady-state fracture permeability. The results indicate that the injection-induced slip can cause a substantial temporary increase in transient fracture permeability, which could considerably facilitate fluid flow. This transient permeability enhancement appears to be much more significant than the relatively minor changes (~1.5 times) in steady-state fracture permeability before each injection experiment (Table S3 in Supporting Information S1). The synchronicity of the changes in transient permeability and slip velocity, signified by the high correlation coefficient (Asuero et al., 1988, 2006), further suggests that the transient permeability enhancement

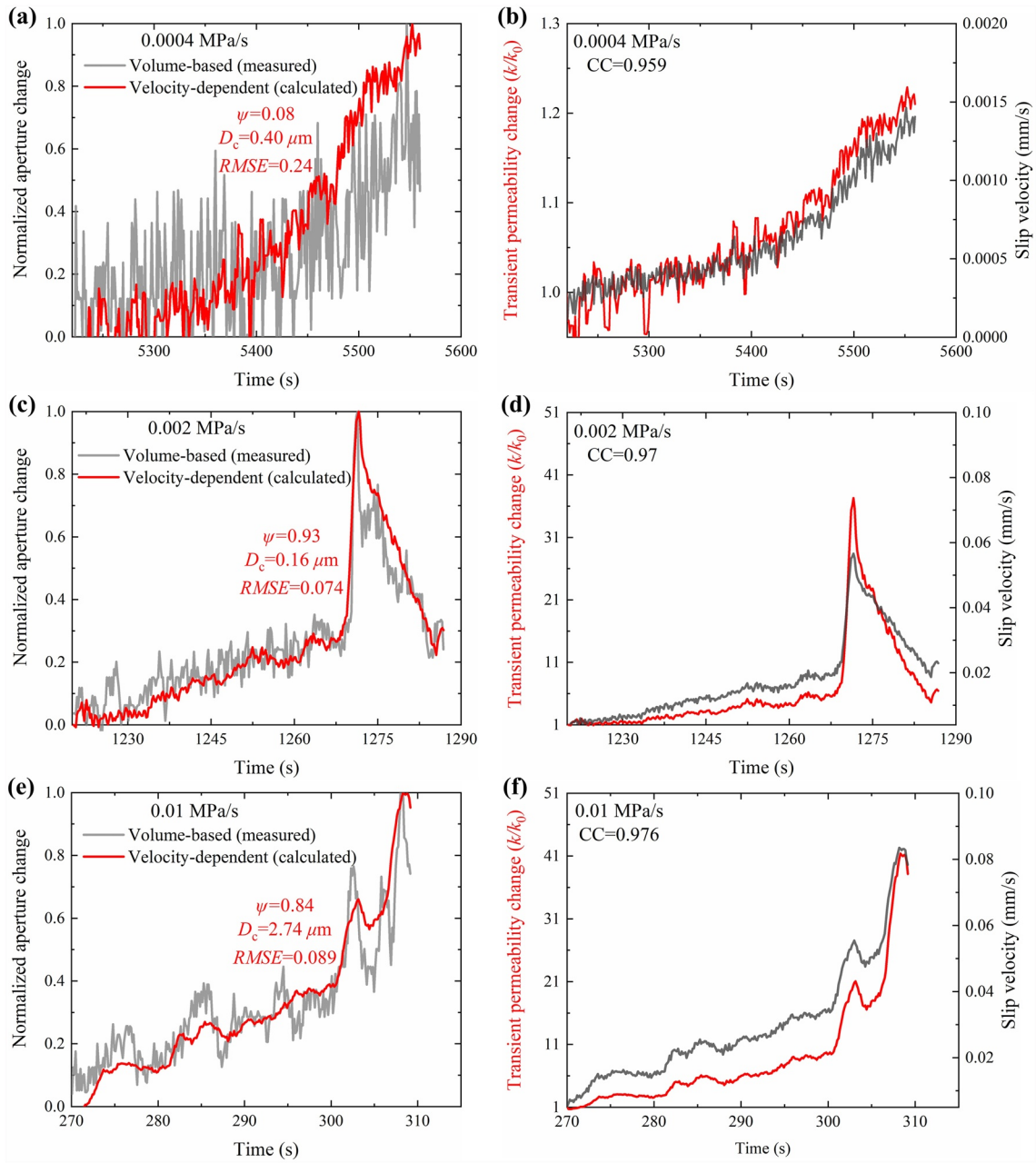

Figure 3. Transient evolution of normalized aperture change (measured and calculated), permeability change and slip velocity during fracture slip in the fluid injection experiments. Results of experiments performed at a pressurization rate of (a and b) 0.0004, (c and d) 0.002, and (e and f) 0.01 MPa/s. The aperture change is normalized with respect to the maximum value in each experiment. Ψ, D_c and root mean square error (RMSE) represent the dilation factor, critical slip distance and RMSE, respectively. The correlation coefficients (CC) between transient permeability change and slip velocity in the three experiments are all close to unity, suggesting the dominant control of slip velocity on the transient permeability change.

is dominantly regulated by the injection-induced slip velocity (Figures 3b, 3d, and 3f). In addition, the primary control of slip velocity on the change of transient permeability is reaffirmed by Figure S5 in Supporting Information S1. This figure demonstrates a consistent rise in transient permeability enhancement corresponding to higher slip velocities, and the rate of increase is primarily controlled by the dilation factor (Ψ) and critical slip distance (D_c).

Figure 4 illustrates that the transient permeability enhancement is evidently not controlled by the slip displacement change, in line with previous results on permeable in-situ faults (Cappa, Guglielmi, & De Barros, 2022).

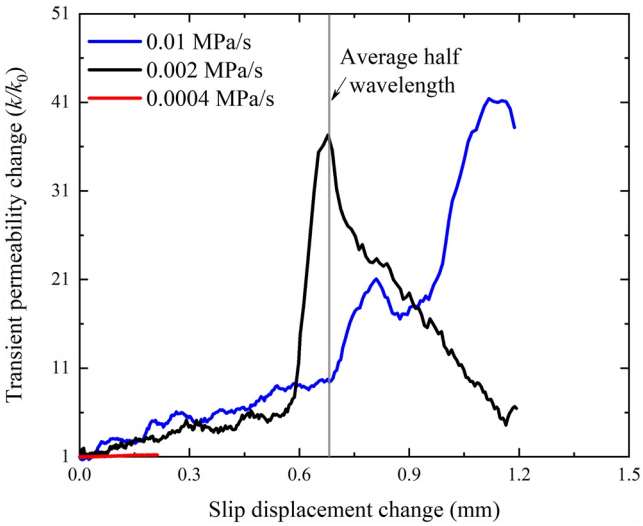

Figure 4. Transient permeability change (k/k_0) against slip displacement change during fracture slip in the fluid injection experiments. A higher fluid pressurization rate tends to promote the transient permeability enhancement at smaller slip displacement changes, while this trend is influenced by fracture surface asperities when the slip displacement change exceeds the average half wavelength of asperity unevenness (~0.68 mm in this study).

In particular, the transient permeability enhancement in the first ~0.24 mm slip displacement is larger at higher pressurization rates. However, the transient permeability enhancement in the case at 0.002 MPa/s starts to exceed that of the case at 0.01 MPa/s at ~0.6 mm slip displacement before dropping lower at ~0.9 mm, followed by the increasing divergence of the transient permeability enhancement in the two cases. The evolution of transient permeability enhancement with slip displacement change shows a similar trend to slip velocity in the three cases (Figure S2 in Supporting Information S1), reconfirming that the rate of increase of transient permeability change with slip displacement is dictated by slip velocity. Since transient permeability enhancement is mainly regulated by slip velocity, its fluctuations likely stem from variations in slip velocity, which can be linked to diverse asperity strengths and sizes (Goebel et al., 2012; Xu et al., 2023; Ye & Ghassemi, 2020). Particularly, the central roughness profile of the fracture surface is characterized by larger-sized waviness and smaller-sized unevenness (Li et al., 2019; Zou et al., 2015; Text S5 and Figure S6 in Supporting Information S1). As we observed an increase in slip displacement up to 1.34 mm within our experimental scope, the primary influencer of frictional resistance alteration is the unevenness of asperities, characterized by an average wavelength of ~1.36 mm (Text S5 and Figure S6 in Supporting Information S1). Previous studies suggest that the frictional resistance can change over a slip displacement of less than half the wavelength of unevenness (approximately ~0.68 mm in our case) due to surface wear effects (Li et al., 2015). In our experiments, indications of surface wear are apparent (Figure S7 in Supporting Information S1). This implies that a slip displacement of approximately ~0.68 mm or beyond would be sufficient to initiate diverse fluctuations in frictional resistance, depending on sizes and strengths of unevenness of asperities. Consequently, these fluctuations would impact both slip velocity and transient permeability. Given the uncertainties involved in determining the average half wavelength of asperity unevenness, the close proximity of 0.68 mm to the observed slip displacement of ~0.6 mm exhibiting a significant fluctuation further supports this interpretation. That is, our results demonstrate that increasing the fluid pressurization rate can enhance transient permeability in our experimental case, suggesting that fluid pressurization rate can promote the transient permeability enhancement by causing faster slip velocity, with concurrent modulations of surface asperities as the slip displacement increases.

4. Discussion

This study has demonstrated that increasing the rate of fluid pressurization can enhance the transient permeability increase, with fluctuations modulated by surface asperities, during fracture slip in triaxial shear-flow experiments with direct fluid injection to the fracture. Our results were obtained on a natural rough fracture without initial filling material in granite under a pre-stressed state. It is important to note that our experiments represent a case where the fracture has a high initial permeability and a slight velocity-strengthening frictional behavior favoring aseismic slip during the fluid injection. The presented results support the hypothesis that the fluid pressurization rate and fracture surface asperities have a significant influence on the transient permeability evolution in a single deformable natural fracture and confirm that the slip velocity dependency of transient fracture permeability previously observed in the laboratory (Fang et al., 2017) and in situ (Cappa, Guglielmi, & De Barros, 2022) is a key process for fluid transport in fractures and faults. Nevertheless, it is important to highlight that our findings are particularly relevant to shallow aseismic slip and the accompanying changes in transient permeability, even though they might not comprehensively encompass the entire steady-state range. These results could also offer valuable insights into the understanding of permeability evolution associated with tremors occurring at greater depths due to slow slip events (cf., Guglielmi et al., 2015).

The excellent agreement between the experimental data and the numerical solutions highlights that the velocity dependency of transient fracture permeability is a dominant process during injection. Although we obtained a good fit to data with the velocity-dependent aperture model, other mechanisms may also influence the fracture's hydromechanical responses. In our experiments, the clogging and unclogging of fluid pathways associated

with flux-driven particle mobilization (Candela et al., 2014) may only have a minimal impact on the transient permeability changes. Indeed, we observed that the root mean square asperity height and peak-to-trough distance decrease by only 0.74 and 0.68 mm, respectively, after the experiments (Table S2 in Supporting Information S1). Given that the average grain size of the granite is approximately 2 mm (Li et al., 2020), we infer that the fracture surface primarily underwent surface wear (Figure S7 in Supporting Information S1), rather than significant grain detachments. This observation also guarantees that the results of the three consecutive fluid injection experiments on the same natural rough fracture can be reasonably used for comparison to explore the effects of pressurization rate and surface asperities, which is also supported by the negligible reduction of JRC from 12.5 before the experiments to 12.4 after the experiments (see Table S2 in Supporting Information S1 and the notes below). The insignificant surface damage after the experiments could be due to the low effective normal stress (σ'_n) relative to the uniaxial compressive strength of the host rock (i.e., $\sigma'_n < 0.1$ UCS, Table S1 in Supporting Information S1), which prevents the occurrence of severe asperity breakages (cf., Ji et al., 2021; Li et al., 2022; Oh et al., 2016). Therefore, due to the trivial surface damage and the small amount of small-sized wear particles produced, it is likely that flux-driven particle mobilization did not exert a substantial effect on the transient permeability changes in our experiments. In addition, as opposed to injection-induced slow slip in our experiments, fast stick-slip events may further complicate the transient permeability evolution in the laboratory scale (Almakari et al., 2020; Rutter & Mecklenburgh, 2018). Similarly, in-situ fluid injection experiments on slowly slipping faults also demonstrated that the permeability evolution can be affected by slip modes (i.e., aseismic and seismic) (Cappa, Guglielmi, & De Barros, 2022; Cappa, Guglielmi, Nussbaum, et al., 2022; Guglielmi et al., 2015).

However, when the fracture slip occurs at higher effective pressures (cf., Goebel et al., 2012, 2017, 2023; Ji, Wang, et al., 2022; Ji, Hofmann, Rutter, et al., 2022; Ye & Ghassemi, 2018, 2020), the presence of wear particles and any associated colloidal seal are anticipated to have a notable impact on the transient fracture permeability evolution during fluid injection, in addition to the velocity-dependent process (e.g., Cappa, Guglielmi, & De Barros, 2022). Specifically, the combination of pore throat expansion through shear dilation (cf., Im et al., 2018) and fluid pressure migration during injection (e.g., Ji et al., 2020; Passelègue et al., 2018) is likely to favor the flux-driven unclogging of the fracture, potentially leading to further transient permeability enhancement. Meanwhile, the transition from slow slip to stick-slip failure of fractures could be promoted by elevating effective pressures (e.g., Dieterich, 1978; Scuderi et al., 2016) and reducing the friction rate parameter (e.g., Fang et al., 2017), possibly causing complex transient permeability evolution arising from the cycling between near-zero slip velocity during the stick period and abrupt velocity jump during the dynamic slip period (cf., Almakari et al., 2020; Morad et al., 2022). Additionally, elevating both normal stress and shear stress have the tendency to decrease fracture permeability due to the obstruction of fluid pathways by the produced abrasive particles (Rutter & Mecklenburgh, 2018). Moreover, the ratio of shear stress to shear strength could impact the slip velocity during injection-induced slip (Passelègue et al., 2018), potentially promoting aperture changes facilitated by velocity augmentation. Nonetheless, the interaction between the flux-driven particle mobilization and the intricate permeability evolution resulting from complex slip modes remains uncertain. Consequently, there is a need to explore the transient evolution of permeability during fluid injection at elevated effective pressures and diverse shear stress levels in fractures with different roughnesses and exhibiting a range of frictional properties and slip modes.

In terms of scales, laboratory fractures in this study represents a fracture of zero or low effective fracture toughness and cohesion, which discounts the crack propagation-induced permeability change (Abe & Horne, 2023; Abe et al., 2021; Ye & Ghassemi, 2019), which are clearly idealizations of the complexity of natural fracture networks. Thus, at the reservoir-scale fracture network, the transient permeability change of individual fractures can be complicated by fracture surface topography and infilling, fracture interactions and connectivity, stress state, rock type, as well as the decoupling of fracture slip and opening in the case of initially low-permeability fractures (Cappa, Guglielmi, Nussbaum, et al., 2022; Rutter & Hackston, 2017). Clearly, fracture permeability during fluid injection is a fast-evolving property significantly affected by different processes that are difficult to compare across scales. To further bridge the scale gap, our results obtained from lab-scale single fracture experiments with the centimeter scale need to be extended for mine- and reservoir- scale injection experiments, in which increasing pressure gradients can also alter the flow-through area of a heterogeneous fracture/fault.

Beyond improving the fundamental understanding of the process of fracture permeability enhancement controlled by pressurization rate and surface asperities, the mechanism observed in this lab-scale experiment can be useful for implementing permeability enhancement and seismicity mitigation in the reservoir scale. The transient permeability increases in the pressurized zone upon local slip may accelerate fluid flow in mainly the fault-parallel

direction and the rapid transfer of high pressure at distance from the fluid source. Moreover, as shown in previous studies, high-rate fluid pressurization could enhance the seismic hazard (e.g., Goebel & Shirzaei, 2020; Ji, Wang, et al., 2022; Ji & Wu, 2020; Passelègue et al., 2018; Rudnicki & Zhan, 2020; Wang et al., 2020). Thus, the competition between pressurization and frictional processes in fracture/fault stability is a dominant factor in the trade-off between increasing reservoir permeability and the mitigative impact of slowing or ceasing injection on seismic hazard.

5. Conclusions

Our fluid injection experiments on a pre-stressed natural fracture with high initial permeability have demonstrated that injecting fluid into fractures with a slightly velocity-strengthening frictional behavior leads to slow slipping and a significant transient increase in permeability. The permeability can reach up to approximately 41 times its initial value when the maximum slip velocity of 0.085 mm/s is achieved through high-rate fluid injection. We have identified that the change in hydraulic aperture due to slip velocity is the primary factor driving the temporary evolution of fracture permeability, and this effect is modulated by fluid pressurization rate and fracture surface asperities. These findings highlight the potential to engineer permeability evolution for subsurface geoenergy applications by controlling the fluid pressurization rate specifically on slowly slipping fractures.

Notation

JRC	joint roughness coefficient
RMS	root mean square
RMSE	root mean square error
UCS	uniaxial compressive strength
A	area of the elliptical fracture
b	hydraulic aperture
b_0	initial hydraulic aperture
b^n_{evo}	modeled aperture at the nth velocity step
b^n_{slip}	slip-dependent aperture at the nth velocity step
d	slip displacement change
D_c	critical slip distance
k	fracture permeability
k_0	initial fracture permeability
k_n	transient fracture permeability at the nth velocity step
p	fluid pressure
v	slip velocity
v_0	background slip velocity
Δb	transient change of hydraulic aperture
ΔV_f	additional injected fluid volume caused by fracture slip
$\Delta\varepsilon$	dilation parameter
μ	friction coefficient
σ_n	normal stress
σ'_n	effective normal stress
τ_p	peak shear strength
Ψ	dilation factor

Data Availability Statement

This manuscript is accompanied by Supporting Information S1. The experimental data generated in this study are available at https://figshare.com/s/2fa49f5a2240aff4785e, and the Python code for the numerical inversion is freely available via https://github.com/Ranger-boop/Inversion_of_aperture_changes_accompanying_injection-induced_fracture_slip.

Acknowledgments
We would like to thank Thomas H. W. Goebel and an anonymous reviewer for many valuable comments and suggestions that helped to improve the original manuscript. This work is financially supported by the Helmholtz Association's Initiative and Networking Fund for the Helmholtz Young Investigator Group ARES (contract VH-NG-1516). This material is based on a part of the PhD work of the first author, and thus the first author acknowledges the PhD Research Scholarship from Nanyang Technological University (NTU), Singapore. Open Access funding enabled and organized by Projekt DEAL.

References

Abe, A., & Horne, R. N. (2023). Investigating fracture network creation and stimulation mechanism of EGS reservoirs. *Geothermics*, *107*, 102606. https://doi.org/10.1016/j.geothermics.2022.102606

Abe, A., Kim, T. W., & Horne, R. N. (2021). Laboratory hydraulic stimulation experiments to investigate the interaction between newly formed and preexisting fractures. *International Journal of Rock Mechanics and Mining Sciences*, *141*, 104665. https://doi.org/10.1016/j.ijrmms.2021.104665

Almakari, M., Chauris, H., Passelègue, F., Dublanchet, P., & Gesret, A. (2020). Fault's hydraulic diffusivity enhancement during injection induced fault reactivation: Application of pore pressure diffusion inversions to laboratory injection experiments. *Geophysical Journal International*, *223*(3), 2117–2132. https://doi.org/10.1093/gji/ggaa446

Ashman, I. R., & Faulkner, D. R. (2023). The effect of clay content on the dilatancy and frictional properties of fault gouge. *Journal of Geophysical Research: Solid Earth*, *128*(4). https://doi.org/10.1029/2022jb025878

Asuero, A. G., Gonzalez, G., de Pablos, F., & Ariza, J. L. (1988). Determination of the optimum working range in spectrophotometric procedures. *Talanta*, *35*(7), 531–537. https://doi.org/10.1016/0039-9140(88)80127-9

Asuero, A. G., Sayago, A., & González, A. G. (2006). The correlation coefficient: An overview. *Critical Reviews in Analytical Chemistry*, *36*(1), 41–59. https://doi.org/10.1080/10408340500526766

Barton, C., Moos, D., & Tezuka, K. (2009). Geomechanical wellbore imaging: Implications for reservoir fracture permeability. *AAPG Bulletin*, *93*(11), 1551–1569. https://doi.org/10.1306/06180909030

Barton, N., & Choubey, V. (1977). The shear strength of rock joints in theory and practice. *Rock Mechanics*, *10*(1–2), 1–54. https://doi.org/10.1007/bf01261801

Brady, B. H., & Brown, E. T. (2013). *Rock mechanics: For underground mining*. Springer Science & Business Media.

Byerlee, J. D. (1978). Friction of rocks. *Pure and Applied Geophysics*, *116*(4), 615–626. https://doi.org/10.1007/bf00876528

Candela, T., Brodsky, E. E., Marone, C., & Elsworth, D. (2014). Laboratory evidence for particle mobilization as a mechanism for permeability enhancement via dynamic stressing. *Earth and Planetary Science Letters*, *392*, 279–291. https://doi.org/10.1016/j.epsl.2014.02.025

Cappa, F., Guglielmi, Y., & De Barros, L. (2022). Transient evolution of permeability and friction in a slowly slipping fault activated by fluid pressurization. *Nature Communications*, *13*(1), 3039. https://doi.org/10.1038/s41467-022-30798-3

Cappa, F., Guglielmi, Y., Nussbaum, C., De Barros, L., & Birkholzer, J. (2022). Fluid migration in low-permeability faults driven by decoupling of fault slip and opening. *Nature Geoscience*, *15*(9), 747–751. https://doi.org/10.1038/s41561-022-00993-4

Das, I., & Zoback, M. D. (2013). Long-period, long-duration seismic events during hydraulic stimulation of shale and tight-gas reservoirs-Part 1: Waveform characteristics LPLD events: Waveform characteristics. *Geophysics*, *78*(6), KS107–KS118.

Dieterich, J. H. (1978). Time-dependent friction and the mechanics of stick-slip. *Pure and Applied Geophysics*, *116*(4–5), 790–806. https://doi.org/10.1007/bf00876539

Fang, Y., Elsworth, D., Ishibashi, T., & Zhang, F. (2018). Permeability evolution and frictional stability of fabricated fractures with specified roughness. *Journal of Geophysical Research: Solid Earth*, *123*(11), 9355–9375. https://doi.org/10.1029/2018jb016215

Fang, Y., Elsworth, D., Wang, C., Ishibashi, T., & Fitts, J. P. (2017). Frictional stability-permeability relationships for fractures in shales. *Journal of Geophysical Research: Solid Earth*, *122*(3), 1760–1776. https://doi.org/10.1002/2016jb013435

Fang, Y., Elsworth, D., Wang, C., & Jia, Y. (2018). Mineralogical controls on frictional strength, stability and shear permeability evolution of fractures. *Journal of Geophysical Research: Solid Earth*, *123*(5), 3549–3563. https://doi.org/10.1029/2017jb015338

Goebel, T. H. W., Becker, T. W., Schorlemmer, D., Stanchits, S., Sammis, C., Rybacki, E., & Dresen, G. (2012). Identifying fault heterogeneity through mapping spatial anomalies in acoustic emission statistics. *Journal of Geophysical Research*, *117*(B3), B03310. https://doi.org/10.1029/2011JB008763

Goebel, T. H. W., Brodsky, E. E., & Dresen, G. (2023). Fault roughness promotes earthquake-like aftershock clustering in the lab. *Geophysical Research Letters*, *50*(8), e2022GL101241. https://doi.org/10.1029/2022gl101241

Goebel, T. H. W., Kwiatek, G., Becker, T. W., Brodsky, E. E., & Dresen, G. (2017). What allows seismic events to grow big? Insights from b-value and fault roughness analysis in laboratory stick-slip experiments. *Geology*, *45*(9), 815–818. https://doi.org/10.1130/g39147.1

Goebel, T. H. W., & Shirzaei, M. (2020). More than 40 yr of potentially induced seismicity close to the San Andreas fault in San Ardo, Central California. *Seismological Research Letters*, *92*(1), 187–198. https://doi.org/10.1785/0220200276

Guglielmi, Y., Cappa, F., Avouac, J.-P., Henry, P., & Elsworth, D. (2015). Seismicity triggered by fluid injection–induced aseismic slip. *Science*, *348*(6240), 1224–1226. https://doi.org/10.1126/science.aab0476

Gutierrez, M., Øino, L. E., & Nygård, R. (2000). Stress-dependent permeability of a de-mineralised fracture in shale. *Marine and Petroleum Geology*, *17*(8), 895–907. https://doi.org/10.1016/S0264-8172(00)00027-1

Holland, J. H. (1992). *Adaptation in natural and artificial systems: An introductory analysis with applications to biology, control, and artificial intelligence*. MIT Press.

Im, K., Elsworth, D., & Fang, Y. (2018). The influence of pre-slip sealing on the permeability evolution on fractures and faults. *Geophysical Research Letters*, *45*(1), 166–175. https://doi.org/10.1002/2017gl076216

Ishibashi, T., Elsworth, D., Fang, Y., Riviere, J., Madara, B., Asanuma, H., et al. (2018). Friction-stability-permeability evolution of a fracture in granite. *Water Resources Research*, *54*(12), 9901–9918. https://doi.org/10.1029/2018WR022598

Jalali, M., Gischig, V., Doetsch, J., Näf, R., Krietsch, H., Klepikova, M., et al. (2018). Transmissivity changes and microseismicity induced by small-scale hydraulic fracturing tests in crystalline rock. *Geophysical Research Letters*, *45*(5), 2265–2273. https://doi.org/10.1002/2017gl076781

Ji, Y. (2020). *Shear-flow characteristics of rock fractures and implications for injection-induced seismicity*. Ph. D. Nanyang Technological University.

Ji, Y., Hofmann, H., Duan, K., & Zang, A. (2022). Laboratory experiments on fault behavior towards better understanding of injection-induced seismicity in geoenergy systems. *Earth-Science Reviews*, *226*, 103916. https://doi.org/10.1016/j.earscirev.2021.103916

Ji, Y., Hofmann, H., Rutter, E. H., Xiao, F., & Yang, L. (2022). Revisiting the evaluation of hydraulic transmissivity of elliptical rock fractures in triaxial shear-flow experiments. *Rock Mechanics and Rock Engineering*, *55*(6), 3781–3789. https://doi.org/10.1007/s00603-022-02797-9

Ji, Y., Kluge, C., Hofmann, H., & Blöcher, G. (2022). Effects of external temperature and dead volume on laboratory measurements of pore pressure and injected volume in a rock fracture. *Journal of Rock Mechanics and Geotechnical Engineering*, *14*(5), 1461–1469. https://doi.org/10.1016/j.jrmge.2021.12.007

Ji, Y., Wang, L., Hofmann, H., Kwiatek, G., & Dresen, G. (2022). High-rate fluid injection reduces the nucleation length of laboratory earthquakes on critically stressed faults in granite. *Geophysical Research Letters*, *49*(23), e2022GL100418. https://doi.org/10.1029/2022gl100418

Ji, Y., Wanniarachchi, W. A. M., & Wu, W. (2020). Effect of fluid pressure heterogeneity on injection-induced fracture activation. *Computers and Geotechnics*, *123*, 103589. https://doi.org/10.1016/j.compgeo.2020.103589

Ji, Y., & Wu, W. (2020). Injection-driven fracture instability in granite: Mechanism and implications. *Tectonophysics*, *791*, 228572. https://doi.org/10.1016/j.tecto.2020.228572
Ji, Y., Wu, W., & Zhao, Z. (2019). Unloading-induced rock fracture activation and maximum seismic moment prediction. *Engineering Geology*, *262*, 105352. https://doi.org/10.1016/j.enggeo.2019.105352
Ji, Y., Zhuang, L., Wu, W., Hofmann, H., Zang, A., & Zimmermann, G. (2021). Cyclic water injection potentially mitigates seismic risks by promoting slow and stable slip of a natural fracture in granite. *Rock Mechanics and Rock Engineering*, *54*(10), 5389–5405. https://doi.org/10.1007/s00603-021-02438-7
Keranen, K. M., & Weingarten, M. (2018). Induced seismicity. *Annual Review of Earth and Planetary Sciences*, *46*(1), 149–174. https://doi.org/10.1146/annurev-earth-082517-010054
Kestin, J. (1979). *A course in thermodynamics* (Vol. 1). CRC Press.
Kim, J., & Moridis, G. J. (2015). Numerical analysis of fracture propagation during hydraulic fracturing operations in shale gas systems. *International Journal of Rock Mechanics and Mining Sciences*, *76*, 127–137. https://doi.org/10.1016/j.ijrmms.2015.02.013
Kohli, A. H., & Zoback, M. D. (2013). Frictional properties of shale reservoir rocks. *Journal of Geophysical Research: Solid Earth*, *118*(9), 5109–5125. https://doi.org/10.1002/jgrb.50346
Li, S., & Zhang, D. (2023). Three-dimensional thermoporoelastic modeling of hydrofracturing and fluid circulation in Hot Dry Rock. *Journal of Geophysical Research: Solid Earth*, *128*(2), e2022JB025673. https://doi.org/10.1029/2022jb025673
Li, Y., Du, X., & Ji, Y. (2022). Prediction of the transitional normal stress of rock joints under shear. *International Journal of Rock Mechanics and Mining Sciences*, *159*, 105203. https://doi.org/10.1016/j.ijrmms.2022.105203
Li, Y., Oh, J., Mitra, R., & Hebblewhite, B. (2015). Experimental studies on the mechanical behavior of rock joints with various openings. *Rock Mechanics and Rock Engineering*, *49*(3), 837–853. https://doi.org/10.1007/s00603-015-0781-3
Li, Y., Sun, S., & Tang, C. A. (2019). Analytical prediction of the shear behavior of rock joints with quantified waviness and unevenness through wavelet analysis. *Rock Mechanics and Rock Engineering*, *52*(10), 3645–3657. https://doi.org/10.1007/s00603-019-01817-5
Li, Z., Elsworth, D., Wang, C., Boyd, L., Frone, Z., Metcalfe, E., et al. (2021). Constraining maximum event magnitude during injection-triggered seismicity. *Nature Communications*, *12*(1), 1528. https://doi.org/10.1038/s41467-020-20700-4
Li, Z., Wong, L. N. Y., & Teh, C. I. (2020). Influence of thermal and mechanical loading on development of microcracks in granite. *Rock Mechanics and Rock Engineering*, *53*(5), 2035–2051. https://doi.org/10.1007/s00603-019-02030-0
Marone, C. (1998). Laboratory-derived friction laws and their application to seismic faulting. *Annual Review of Earth and Planetary Sciences*, *26*(1), 643–696. https://doi.org/10.1146/annurev.earth.26.1.643
Mavko, G., Mukerji, T., & Dvorkin, J. (2009). *The rock physics handbook*. Cambridge University Press.
Morad, D., Sagy, A., Tal, Y., & Hatzor, Y. H. (2022). Fault roughness controls sliding instability. *Earth and Planetary Science Letters*, *579*, 117365. https://doi.org/10.1016/j.epsl.2022.117365
Oh, J., Li, Y., Mitra, R., & Canbulat, I. (2016). A numerical study on dilation of a saw-toothed rock joint under direct shear. *Rock Mechanics and Rock Engineering*, *50*(4), 913–925. https://doi.org/10.1007/s00603-016-1142-6
Okazaki, K., Katayama, I., & Noda, H. (2013). Shear-induced permeability anisotropy of simulated serpentinite gouge produced by triaxial deformation experiments. *Geophysical Research Letters*, *40*(7), 1290–1294. https://doi.org/10.1002/grl.50302
Olasolo, P., Juárez, M. C., Morales, M. P., D´Amico, S., & Liarte, I. A. (2016). Enhanced geothermal systems (EGS): A review. *Renewable and Sustainable Energy Reviews*, *56*, 133–144. https://doi.org/10.1016/j.rser.2015.11.031
Passelègue, F. X., Brantut, N., & Mitchell, T. M. (2018). Fault reactivation by fluid injection: Controls from stress state and injection rate. *Geophysical Research Letters*, *45*(23), 12837–812846. https://doi.org/10.1029/2018GL080470
Peng, J., Wong, L. N. Y., & Teh, C. I. (2017). Influence of grain size heterogeneity on strength and micro-cracking behavior of crystalline rocks. *Journal of Geophysical Research: Solid Earth*, *122*(2), 1054–1073. https://doi.org/10.1002/2016jb013469
Rudnicki, J. W., & Zhan, Y. (2020). Effect of pressure rate on rate and state frictional slip. *Geophysical Research Letters*, *47*(21), e2020GL089426. https://doi.org/10.1029/2020GL089426
Rutter, E., & Hackston, A. (2017). On the effective stress law for rock-on-rock frictional sliding, and fault slip triggered by means of fluid injection. *Philosophical Transactions of the Royal Society A: Mathematical, Physical & Engineering Sciences*, *375*(2103), 20160001. https://doi.org/10.1098/rsta.2016.0001
Rutter, E. H., & Mecklenburgh, J. (2017). Hydraulic conductivity of bedding-parallel cracks in shale as a function of shear and normal stress. *Geological Society, London, Special Publications*, *454*(1), 67–84. https://doi.org/10.1144/sp454.9
Rutter, E. H., & Mecklenburgh, J. (2018). Influence of normal and shear stress on the hydraulic transmissivity of thin cracks in a tight quartz sandstone, a granite, and a shale. *Journal of Geophysical Research: Solid Earth*, *123*(2), 1262–1285. https://doi.org/10.1002/2017jb014858
Samuelson, J., Elsworth, D., & Marone, C. (2009). Shear-induced dilatancy of fluid-saturated faults: Experiment and theory. *Journal of Geophysical Research*, *114*(B12), B12404. https://doi.org/10.1029/2008jb006273
Schoenball, M., Ajo-Franklin, J. B., Blankenship, D., Chai, C., Chakravarty, A., Dobson, P., et al. (2020). Creation of a mixed-mode fracture network at mesoscale through hydraulic fracturing and shear stimulation. *Journal of Geophysical Research: Solid Earth*, *125*(12), e2020JB019807. https://doi.org/10.1029/2020jb019807
Schultz, R., Skoumal, R. J., Brudzinski, M. R., Eaton, D., Baptie, B., & Ellsworth, W. (2020). Hydraulic fracturing-induced seismicity. *Reviews of Geophysics*, *58*(3), e2019RG000695. https://doi.org/10.1029/2019RG000695
Scuderi, M. M., Marone, C., Tinti, E., Di Stefano, G., & Collettini, C. (2016). Precursory changes in seismic velocity for the spectrum of earthquake failure modes. *Nature Geoscience*, *9*(9), 695–700. https://doi.org/10.1038/ngeo2775
Snow, D. T. (1969). Anisotropic permeability of fractured media. *Water Resources Research*, *5*(6), 1273–1289. https://doi.org/10.1029/wr005i006p01273
Tinti, E., Scuderi, M. M., Scognamiglio, L., Di Stefano, G., Marone, C., & Collettini, C. (2016). On the evolution of elastic properties during laboratory stick-slip experiments spanning the transition from slow slip to dynamic rupture. *Journal of Geophysical Research: Solid Earth*, *121*(12), 8569–8594. https://doi.org/10.1002/2016jb013545
Wang, L., Kwiatek, G., Rybacki, E., Bonnelye, A., Bohnhoff, M., & Dresen, G. (2020). Laboratory study on fluid-induced fault slip behavior: The role of fluid pressurization rate. *Geophysical Research Letters*, *47*(6), e2019GL086627. https://doi.org/10.1029/2019gl086627
Witherspoon, P. A., Wang, J. S., Iwai, K., & Gale, J. E. (1980). Validity of cubic law for fluid flow in a deformable rock fracture. *Water Resources Research*, *16*(6), 1016–1024. https://doi.org/10.1029/wr016i006p01016
Wu, W., Reece, J. S., Gensterblum, Y., & Zoback, M. D. (2017). Permeability evolution of slowly slipping faults in shale reservoirs. *Geophysical Research Letters*, *44*(22), 11368–311375. https://doi.org/10.1002/2017GL075506
Xu, S., Fukuyama, E., Yamashita, F., Kawakata, H., Mizoguchi, K., & Takizawa, S. (2023). Fault strength and rupture process controlled by fault surface topography. *Nature Geoscience*, *16*(1), 94–100. https://doi.org/10.1038/s41561-022-01093-z

Ye, Z., & Ghassemi, A. (2018). Injection-induced shear slip and permeability enhancement in granite fractures. *Journal of Geophysical Research: Solid Earth*, *123*(10), 9009–9032. https://doi.org/10.1029/2018JB016045

Ye, Z., & Ghassemi, A. (2019). Injection-induced propagation and coalescence of preexisting fractures in granite under triaxial stress. *Journal of Geophysical Research: Solid Earth*, *124*(8), 7806–7821. https://doi.org/10.1029/2019jb017400

Ye, Z., & Ghassemi, A. (2020). Heterogeneous fracture slip and aseismic-seismic transition in a triaxial injection test. *Geophysical Research Letters*, *47*(14), e2020GL087739. https://doi.org/10.1029/2020gl087739

Zang, A., Oye, V., Jousset, P., Deichmann, N., Gritto, R., McGarr, A., et al. (2014). Analysis of induced seismicity in geothermal reservoirs—An overview. *Geothermics*, *52*, 6–21. https://doi.org/10.1016/j.geothermics.2014.06.005

Zangerl, C., Evans, K. F., Eberhardt, E., & Loew, S. (2008). Normal stiffness of fractures in granitic rock: A compilation of laboratory and in situ experiments. *International Journal of Rock Mechanics and Mining Sciences*, *45*(8), 1500–1507. https://doi.org/10.1016/j.ijrmms.2008.02.001

Zbigniew, M. (1996). Genetic algorithms+ data structures= evolution programs. *Computational Statistics*, 372–373.

Zhao, J. (1997). Joint surface matching and shear strength part A: Joint matching coefficient (JMC). *International Journal of Rock Mechanics and Mining Sciences*, *34*(2), 173–178. https://doi.org/10.1016/S0148-9062(96)00062-9

Zhuang, L., & Zang, A. (2021). Laboratory hydraulic fracturing experiments on crystalline rock for geothermal purposes. *Earth-Science Reviews*, *216*, 103580. https://doi.org/10.1016/j.earscirev.2021.103580

Zou, L., Jing, L., & Cvetkovic, V. (2015). Roughness decomposition and nonlinear fluid flow in a single rock fracture. *International Journal of Rock Mechanics and Mining Sciences*, *75*, 102–118. https://doi.org/10.1016/j.ijrmms.2015.01.016

References From the Supporting Information

Cappa, F., Guglielmi, Y., Rutqvist, J., Tsang, C. F., & Thoraval, A. (2006). Hydromechanical modelling of pulse tests that measure fluid pressure and fracture normal displacement at the Coaraze Laboratory site, France. *International Journal of Rock Mechanics and Mining Sciences*, *43*(7), 1062–1082. https://doi.org/10.1016/j.ijrmms.2006.03.006

Cornet, F. H., Li, L., Hulin, J. P., Ippolito, I., & Kurowski, P. (2003). The hydromechanical behavior of a fracture: An in situ experimental case study. *International Journal of Rock Mechanics and Mining Sciences*, *40*(7–8), 1257–1270. https://doi.org/10.1016/s1365-1609(03)00120-5

Hayward, K. S., & Cox, S. F. (2017). Melt welding and its role in fault reactivation and localization of fracture damage in seismically active faults. *Journal of Geophysical Research: Solid Earth*, *122*(12), 9689–9713. https://doi.org/10.1002/2017jb014903

Ishibashi, T., Watanabe, N., Asanuma, H., & Tsuchiya, N. (2016). Linking microearthquakes to fracture permeability change: The role of surface roughness. *Geophysical Research Letters*, *43*(14), 7486–7493. https://doi.org/10.1002/2016gl069478

Ji, Y., Zhang, W., Hofmann, H., Chen, Y., Kluge, C., Zang, A., & Zimmermann, G. (2023). Modelling of fluid pressure migration in a pressure sensitive fault zone subject to cyclic injection and implications for injection-induced seismicity. *Geophysical Journal International*, *232*(3), 1655–1667. https://doi.org/10.1093/gji/ggac416

Schmittbuhl, J., Schmitt, F., & Scholz, C. (1995). Scaling invariance of crack surfaces. *Journal of Geophysical Research*, *100*(B4), 5953–5973. https://doi.org/10.1029/94JB02885

Tembe, S., Lockner, D. A., & Wong, T.-F. (2010). Effect of clay content and mineralogy on frictional sliding behavior of simulated gouges: Binary and ternary mixtures of quartz, illite, and montmorillonite. *Journal of Geophysical Research*, *115*(B3), B03416. https://doi.org/10.1029/2009jb006383

Tse, R., & Cruden, D. (1979). Estimating joint roughness coefficients. *International Journal of Rock Mechanics and Mining Sciences & Geomechanics Abstracts*, *16*(5), 303–307. https://doi.org/10.1016/0148-9062(79)90241-9

Watanabe, N., Hirano, N., & Tsuchiya, N. (2008). Determination of aperture structure and fluid flow in a rock fracture by high-resolution numerical modeling on the basis of a flow-through experiment under confining pressure. *Water Resources Research*, *44*(6), W06412. https://doi.org/10.1029/2006WR005411